Microsystem Technologies 9 (2003) 331–334 © Springer-Verlag 2003
DOI 10.1007/s00542-002-0253-z

Optimization of an electro-thermally and laterally driven microactuator

C.-C. Lee, W. Hsu

Abstract In previous research about thermally and laterally driven microactuators, Guckel et al. proposed a microactuator based on the variable cross sections but the same length of two adjacent beams. Pan and Hsu presented another type of microactuator based on different lengths but the same cross sections of two adjacent beams. Here, a microactuator that combines the traits of those two designs is proposed, optimized, and fabricated. Finite element analysis is performed to obtain the optimal dimensions of the structures when the maximum lateral displacement is achieved. When the air gap is 2 μm, the optimal performance of current design is similar to Guckel's design with optimal dimensions, but it has 65% larger displacement than Pan and Hsu's design at optimal dimensions. For the case of the large air gap beneath the structure (300 μm), the microactuator of current design has more than 25% tip displacement improvement compared to Guckel's or Pan and Hsu's designs. It is also found that the proposed structure is less sensitive to the beam length variations around optimal point no matter in small or large air gap case. Experimental results also verify that the dimension of the air gap affects the thermal boundary condition, so does the performance and optimal architecture of the microactuators.

1
Introduction

Among various driving principles of microactuators, thermally driven ones have the characteristics of long displacement, large force, and low driving voltage. In previous literature about thermally driven microactuators with lateral motion, two types of structures based on the unsymmetrical thermal expansion of two adjacent beams have been presented. Guckel et al. (1992) proposed a microactuator based on the variable cross sections but the same length of two adjacent beams.

Asymmetric expansion resulted from the wider section with less resistive heating but more thermal dissipation. Later Comtois et al. (1997, 1998) modified the microactuators by surface micromachined polysilicon process and assembled them to be an array for various applications. Huang and Lee (1999) developed the analytical model and proposed the optimal dimensions for Guckel's architecture. Pan and Hsu (1997) presented another type of microactuator based on different lengths but the same cross sections of two adjacent beams. The design principle not only increased the asymmetric expansion effect but also made the actuator work even under uniform temperature distribution. Moreover, numerical simulation was performed to optimize the structure in their research. Here, an optimal structure is proposed to combine the traits of the above two designs, different lengths and various cross sections, to enhance the lateral displacement.

2
Concept design

The basic structure design of the microactuator which incorporates the traits of Guckel's and Pan's architectures (Fig. 1a and 1b, respectively) is shown in Fig. 1c. The microactuator consists of a pair of adjacent beams made of the conductive material. The actuation principle is based on the uneven thermal expansions of two adjacent beams, where the beam with larger thermal expansion will bend toward the other beam with smaller thermal expansion laterally. For example, in Guckel's design, when one beam is wider than the other, the wider beam has lower resistance. Then the thermal expansion of the wider beam will be smaller than the other while heating, as shown in Fig. 1a. For Pan and Hsu's design, when one beam is shorter than the other, the short beam will have smaller thermal expansion while heating, as shown in Fig. 1b. In this investigation, our design tries to combine both the length and width effects in one of two adjacent beams, as shown in Fig. 1c, to see if a larger uneven thermal expansion can be achieved. However, the lateral displacement depends on both thermal and mechanical effects. If the length of the short beam decreases, the lateral stiffness of the structure may deteriorate also. Therefore, the lengths of the wider part and flexure part have to be balanced to obtain the maximum displacement. Finite element analysis is used here to determine the optimal dimensions in different operating conditions.

Received: 17 August 2001/Accepted: 3 May 2002

C.-C. Lee, W. Hsu (✉)
Department of Mechanical Engineering,
National Chiao Tung University, 1001 Ta Hsueh Road,
Hsinchu, Taiwan, 30010, Republic of China
E-mail: whsu@cc.nctu.edu.tw

This project was supported by the National Science Council of the Republic of China, NSC89-2218-E009-005. The staffs at Semiconductor Research Center of NCTU are gratefully acknowledged for providing facilities and technical support.

This paper was presented at the Conference of Micro System Technologies 2001 in March 2001.

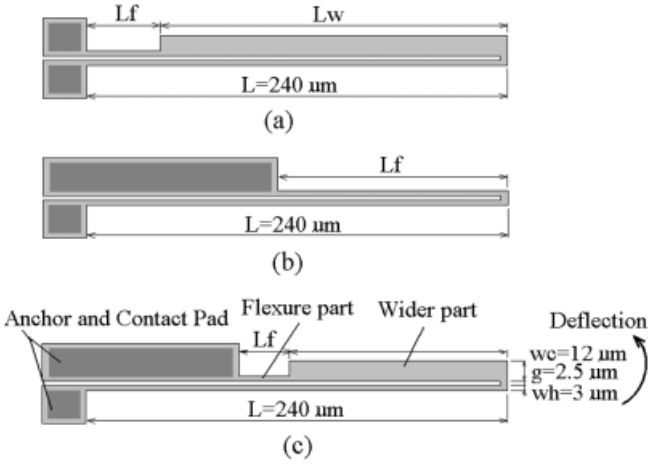

Fig. 1. Schematic view of the three thermally and laterally driven microactuators. **a** Proposed by Guckel et al. 1992; **b** proposed by Pan and Hsu 1997; and **c** current Design

3
Finite element modeling (FEM)

Here, ANSYS5.3 is used to perform electro-thermal-mechanical analysis under the same input voltage first. Also, mechanical properties of the material and related thermal parameters are treated as to be temperature independent in the simulation.

From previous research, the actuator with longer beams leads to larger lateral displacement, but also results in stiction and buckling [Comtois et al. 1997]. On the other hand, considering the thermal effect, wider cold beams leads to larger deflections [Huang and Lee 1999]. For mechanical effect, the wider part of the cold beam can be regarded as the rigid body as long as it is much wider than the flexure part. Also, a smaller gap between two adjacent beams would result in larger deflections [Huang and Lee 1999]. Therefore, the length of the hot beam, the width of the wider part in the cold beam, the gap between two beams, and thickness of the structure are fixed at 240 μm, 12 μm, 2.5 μm, and 2 μm respectively in finite element modeling to have the same basic dimensions in comparison of three designs.

The simulation here will focus on the optimal lengths of flexure (Lf) and wider (Lw) parts in the cold beam to gain maximum lateral displacement under two different air gaps between the substrate and the structures. When the air gap is large, e.g. 300 μm, only the convection effect is considered. When the air gap is small, e.g. 2 μm, the heat conduction from the suspended structures through the air gap to the substrate is also considered. As shown in Fig. 2a, when the underneath air gap is small (2 μm), the optimal dimensions of current design are very closed to Guckel's optimal structure (Lf = 30 μm, Lw = 210 μm). But the tip displacement of the current structure is less sensitive to the length variations of flexure and wider parts. It means the current structure can provide wider length range around optimal point than previous structures. Furthermore, the optimal displacements of Guckel and current designs both are at least 65% larger than Pan and Hsu's design at optimal dimensions (1.5 μm at Lw = 0 and Lf = 100 μm).

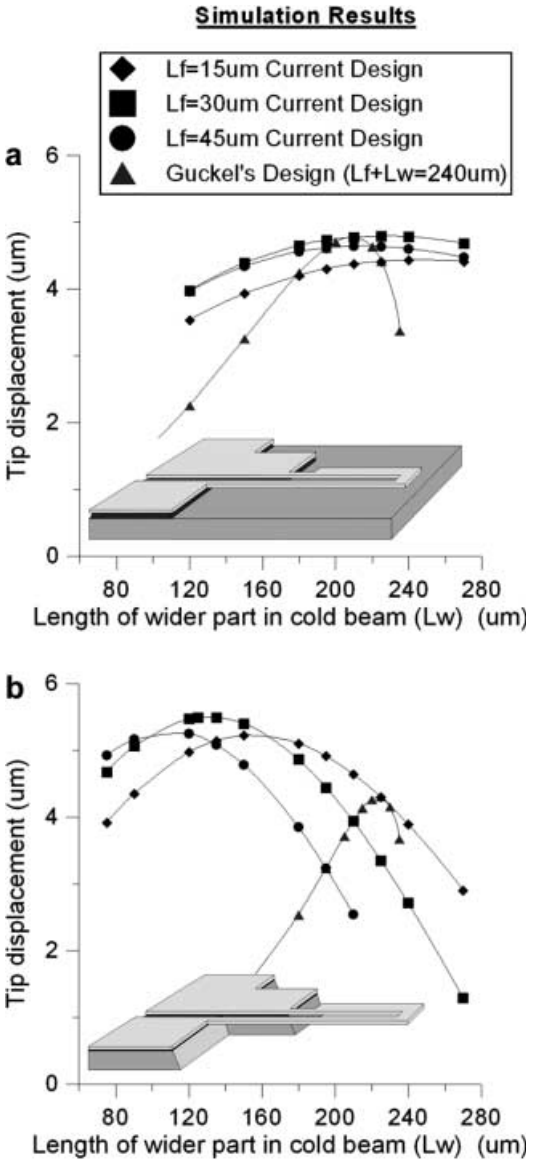

Fig. 2. Simulation results for suspended microactuators with **a** the air gap = 2 μm and input voltage = 5 V; **b** the air gap = 300 μm and input voltage = 3 V

Figure 2b shows the tip displacement of the microactuators with a large air gap under the steady-state simulations. It is found that the microactuator of current design (Lf = 30 μm, Lw = 125 μm) has more than 27% tip displacement compared to Guckel's structure at optimal dimensions (Lf = 15 μm, Lw = 225 μm). Also, the current design has up to 50% more tip displacement than Pan and Hsu's design at optimal dimensions (Lf = 120 μm, Lw = 0), which is not marked in Fig. 2b. Also, performances of three types of microactuators with optimal dimensions are listed in Table 1. It is found that the proposed microactuator still has about 25% larger tip displacement than Guckel's or Pan and Hsu's design under the same input power.

From simulation, it can be found that thermal microactuators with different thermal boundary conditions may lead to various optimal dimensions.

4
Fabrication process

Various dimensions of three types of microactuators, Guckel's, Pan's, and the current design are fabricated in the same chip. The devices for the air gap of 2 μm are achieved by MUMPs [Koester et al. 1994]. For the other case, the fabrication process for the actuators with the large air gap is shown in Fig. 3. First, 0.5 μm thick thermal SiO_2, 0.3 μm thick LPCVD Si_3N_4, and 2 μm LPCVD polysilicon are deposited on a (100) wafer respectively followed by doping phosphorus. Then, the polysilicon is patterned by mask #1 and etched by RIE, as shown in Fig. 3a. Because the silicon substrate underneath the structure will be removed in KOH solution to get a large air gap, the polysilicon layer needs proper protection. Therefore, 0.2 μm thick LPCVD Si_3N_4 is deposited and patterned by mask #2 (Fig. 3b). Then, the wafer is immersed in 25 wt% KOH solution at 70 °C to perform the bulk micromachining process. In such a way, the microstructure is fully released. Finally, the passive layer is removed and the microactuators are finished, as shown in Fig. 3c.

Table 1. Performances of three microactuators under the constant input voltage and constant input power with the larger air gap

	Displacement under constant voltage	Displacement under constant power
Guckel's optimal design (Lf = 15 μm, Lw = 225 μm)	4.30 μm	4.30 μm
Pan and Hsu's optimal design (Lf = 120 μm, Lw = 0 μm)	3.62 μm	4.18 μm
Current optimal design (Lf = 30 μm, Lw = 125 μm)	5.49 μm	5.30 μm

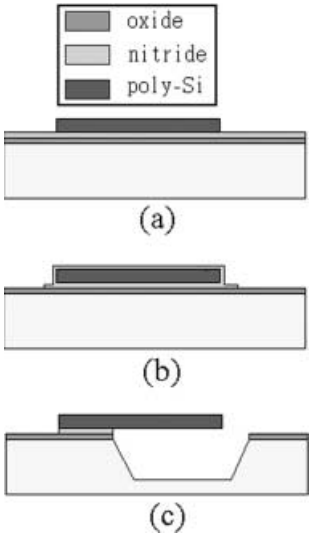

Fig. 3a–c. The fabrication process for microactuators with the large air gap (300 μm)

As Fig. 4 shows, all devices with the air gap of 2 μm are fabricated by MUMPs in the same chip with different dimensions. For microactuators with the large air gap, Fig. 5 shows one of the fabricated actuators of the current design, and the substrate below the actuator is removed by bulk micromachining to obtain the large air gap. Due to the limitation of this fabrication method, part of the contact pad connected to the shorter beam is suspended. Therefore, the fabricated architecture of the large air gap is not exactly the same as the architecture in simulation where all regions of the contact pads are embedded in the substrate, as the architecture shown in Fig. 2b. This difference will lead to different thermal boundary condition, which may result in different performance of the microactuators.

5
Testing results

The tip displacements of the microactuators are recorded by the CCD camera mounted on the probe station, and the measurement error is ±0.3 μm. The input voltages are 5 V and 3 V for microactuators with the small and large air gaps, respectively, as the specifications in simulations. The measurement results are plotted in Fig. 6a and 6b. The air gap condition in the measurement is also shown in the figures. It should be noted that the suspended condition of the architecture in Fig. 6b is not exactly the same as the one in simulation of Fig. 2b.

Figure 6a shows the measurement results for different designs with the small air gaps. It is found that the maximum tip displacement of the current design is very close to Guckel's design. Also, they are both much larger than Pan and Hsu's optimum design, which is not marked in the Fig. 6a. Moreover, the trend in testing results for small air gap is consistent with the simulation results shown in Fig. 2a.

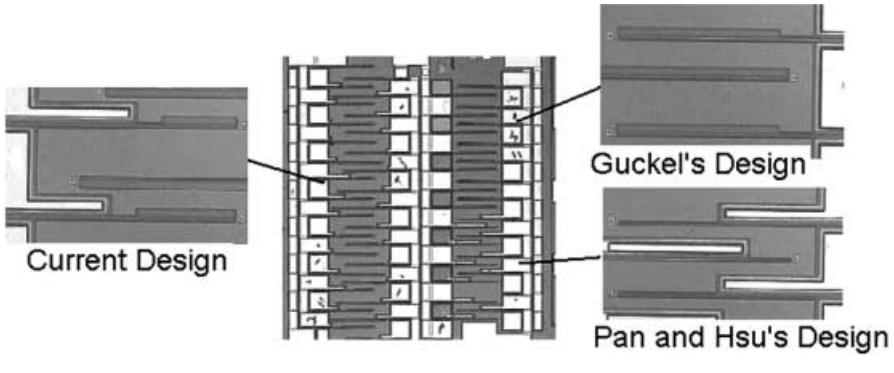

Fig. 4. Three types of microactuators with the small air gap fabricated by MUMPs in the same chip

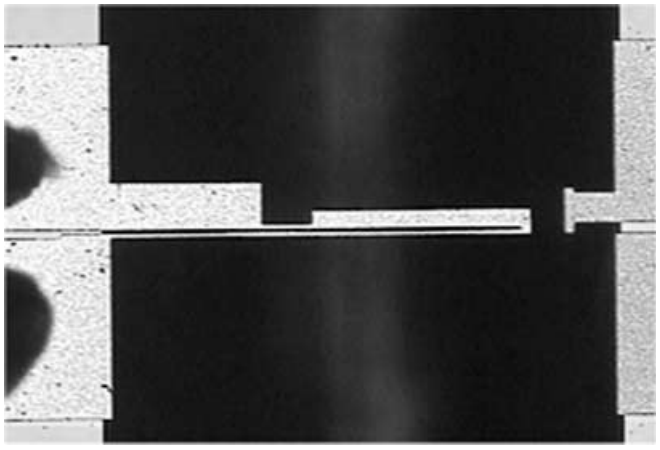

Fig. 5. One of the fabricated actuators of the current design with the large air gap

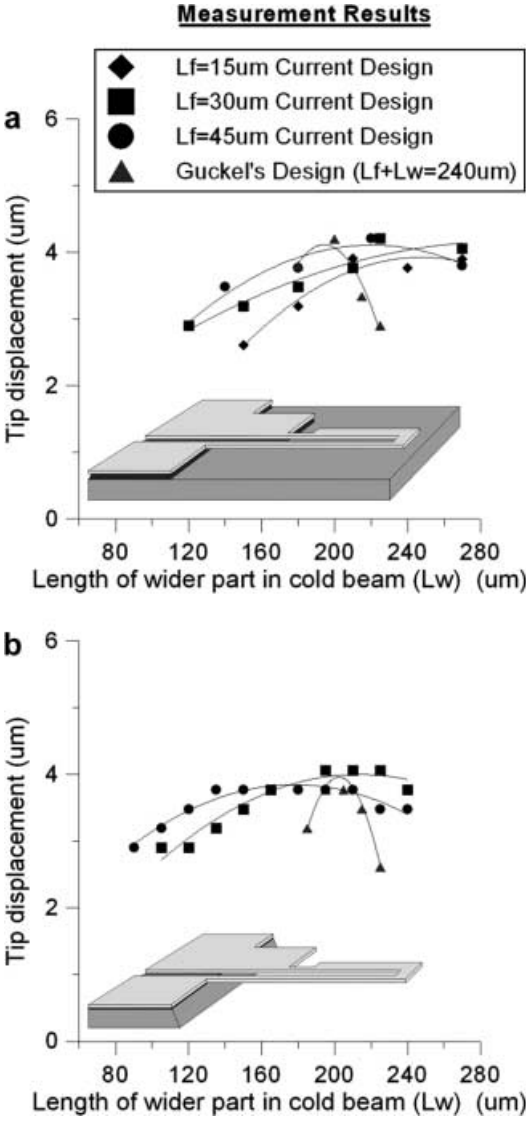

Fig. 6. The measured tip displacements of suspended microactuators with **a** the air gap = 2 μm and input voltage = 5 V; **b** the large air gap = 300 μm and input voltage = 3 V

For the case of the large gap, the measurement results are shown in Fig. 6b. The optimal performance in testing data is not as high as prediction. It is caused by the difference in suspended conditions between fabricated and simulated architectures. Since part of the contact pad connected to the short beam is suspended in the fabricated microactuators, the heat-sink effect close to the short beam is reduced, so is the performances of the microactuators. Even though, the measurement results still verify that a large air gap can change thermal boundary conditions and the behavior of the microactuator. It is also found that the power consumption with a large air gap is only one fifth of the power consumption with a small air gap to achieve the same tip displacement at the optimal dimension. Furthermore, from simulation and testing results, the proposed microactuator is shown to be less sensitive to the beam length variations around the optimal point, no matter in small or large air gap case.

6
Conclusion

An optimal design of a thermally and laterally driven microactuator to combine both the beam length and width effects is proposed here. The tip displacements for three types of microactuators are optimized, fabricated, and compared under the same input voltage and power conditions. When the air gap is 2 μm, the optimal performance of current design is similar to Guckel's design with optimal dimensions. Also, it has a 65% larger displacement than Pan and Hsu's designs at optimal dimensions. For the case of the large gap, the simulation results indicate that the current optimal design can enhance the performance by more than 25%, compared to the other two designs. Although the fabricated architecture with the large air gap is not exactly the same as the architecture in simulation, the experimental results of the actuator with the suspended contact pad can still verify that various thermal boundary conditions may affect the performance and optimal architecture of the microactuators. Also, a larger air gap can efficiently reduce the power consumption of the microactuators. Furthermore, the tip displacement of the current design is less sensitive to the beam length variations on flexure and wider parts, which can give us a wider design range in dimensions.

References

Comtois JH; Bright VM (1997) Applications for surface-micromachined polysilicon thermal actuators and arrays. Sensors and Actuators A58: 19–25

Comtois JH; Michalicek MA; Barron CC (1998) Electrothermal actuators fabricated in four-level planarized surface micromachined polycrystalline silicon. Sensors and Actuators A70: 23–31

Guckel H; Klein J; Christen T; Skrobis K; Landon M; Lovell EG (1992) Thermo-magnetic metal flexure actuators. Technical Digest, IEEE Solid State Sensor and Actuator Workshop, Hilton Head Island, SC: 73–75

Huang Q; Lee NKS (1999) Analysis and design of polysilicon thermal flexure actuator. J Micromech Microeng 9: 64–70

Koester D; Mahedevan R; Marcus K (1994) Multi-User MEMS Processes (MUMPs) Introduction and Design Rules. Rev.3. MCNC MEMS Technology Applications Center, Research Triangle Park, NC, USA

Pan CS; Hsu W (1997) An electro-thermally and laterally driven polysilicon microactuator. J Micromech Microeng 7: 7–13